Journal of *Marine Science and Engineering*

MDPI

Article

Deep Learning-Based Geomorphic Feature Identification in Dredge Pit Marine Environment

Wenqiang Zhang [1,2,*], Xiaobing Chen [3], Xiangwei Zhou [3], Jianhua Chen [4], Jianguo Yuan [5], Taibiao Zhao [4] and Kehui Xu [1,2,*]

[1] Sediment Dynamic Lab, Energy, Coast and Environment Building, Department of Oceanography and Coastal Sciences, Louisiana State University, Baton Rouge, LA 70803, USA
[2] Coastal Studies Institute, Louisiana State University, Baton Rouge, LA 70803, USA
[3] Division of Electrical and Computer Engineering, Louisiana State University, Baton Rouge, LA 70803, USA; xchen87@lsu.edu (X.C.); xwzhou@lsu.edu (X.Z.)
[4] Division of Computer Science and Engineering, Louisiana State University, Baton Rouge, LA 70803, USA; cschen@lsu.edu (J.C.); tzhao3@lsu.edu (T.Z.)
[5] Department of Oceanography and Coastal Sciences, Louisiana State University, Baton Rouge, LA 70803, USA; jyuan8@lsu.edu
* Correspondence: wzhan46@lsu.edu (W.Z.); kxu@lsu.edu (K.X.)

Abstract: Deep learning methods paired with sidescan sonar (SSS) are commonly used in underwater search-and-rescue operations for drowning victims, wrecks, and airplanes. However, these techniques are primarily used to detect mine-like objects and are rarely applied to identifying features in dynamic dredge pit environments. In this study, we present a Sandy Point dredge pit (SPDP) dataset, in which high-resolution SSS data were collected from the west flank of the Mississippi bird-foot delta on the Louisiana inner shelf. This dataset contains a total of 385 SSS images. We then introduce a new Effective Geomorphology Classification model (EGC). Through ablation studies, we analyze the utility of transfer learning on different model architectures and the impact of data augmentations on model performance. This EGC model makes geomorphic feature identification in dredge pit environments, which requires extensive experience and professional knowledge, a quick and efficient task. The combination of SSS images and the EGC model is a cost-effective and valuable toolkit for hazard monitoring in marine dredge pit environments. The SPDP SSS image dataset, especially the feature of pit walls without a rotational slump, is also valuable for other machine learning models.

Keywords: sidescan; sonar; geomorphology; deep learning; coastal restoration; EfficientNet

Citation: Zhang, W.; Chen, X.; Zhou, X.; Chen, J.; Yuan, J.; Zhao, T.; Xu, K. Deep Learning-Based Geomorphic Feature Identification in Dredge Pit Marine Environment. *J. Mar. Sci. Eng.* **2024**, *12*, 1091. https://doi.org/10.3390/jmse12071091

Academic Editor: Giorgio Anfuso

Received: 20 May 2024
Revised: 18 June 2024
Accepted: 26 June 2024
Published: 28 June 2024

1. Introduction

Barrier islands play a critical role in safeguarding inland wetlands and preserving estuarine conditions [1]. The barrier islands within the Mississippi River delta plain are facing rapid deterioration due to a combination of factors, including a significant relative sea-level rise of approximately 0.9 cm/year, a shortage of coastal sand supply, and erosion from storm-induced waves and currents [2–5]. These challenges have been extensively documented over the past decades, highlighting coastal islands' vulnerability and the pressing need for conservation efforts [6–8].

Dredging, recognized globally as a critical excavation activity, entails the extraction and transfer of sediments from the beds of oceans, rivers, and lakes. This process serves multiple purposes, ranging from the creation and enhancement of maritime infrastructure such as harbors, waterways, and dikes to coastal restoration and protection and land reclamation efforts. Additionally, dredging is integral to flood and storm mitigation, the harvesting of minerals for infrastructure projects, and the remediation of contaminated sediments. This is detailed in various studies, including references [9–14]. Specifically, dredging activities on the inner Louisiana continental shelf are of notable economic and

societal importance, with over 50,000 km of pipelines on the Gulf of Mexico's seabed. The Energy Information Administration highlights the Gulf of Mexico's (GOM) substantial contribution to the U.S. 's offshore oil and natural gas production, alongside its pivotal role in housing a significant portion of the country's petroleum refining and natural gas processing capacities. Therefore, landslide monitoring is significant for sediment and energy management.

Synthesizing historical data and continuously monitoring the pits have been of interest to mineral resource managers and decision makers [15–19]. Conventional approaches to analyzing the pre-dredging, dredging, and post-dredging phases incorporate a variety of techniques, such as geophysical surveys (including bathymetric, subbottom, and sidescan), sediment sampling through corings and grabs, water analysis, and continuous monitoring with optical and acoustic sensors [19,20]. These methods are complemented by profiling and ship-based transects, among others. While coring and geophysical surveys are effective in identifying sediment characteristics, they often come with constraints regarding spatial coverage and high survey costs. Sediment coring, although accurate for ground-truthing conditions on the seabed, is notably time-intensive and requires significant labor, typically executed intermittently over extended periods (for example, during seasonal studies) [21]. Multi-beam bathymetric surveys offer detailed insights into morphological changes but are expensive, leading to infrequent monitoring of many dredge sites, possibly only once every few years [20,22,23]. In contrast, sidescan sonar, with its broader survey range, stands out as a potential cost-effective method for identifying various sediment substrates, including rocky terrains, wrecks, oyster beds, sand, and mud, demonstrating its versatility and efficiency in marine substrate detection [20,24,25].

Machine learning (ML) has emerged as a pivotal technology in the enhancement of feature identification within sidescan sonar imagery, a critical tool for underwater exploration—including seabed types, marine habitats, archaeological sites, and man-made objects like shipwrecks and debris—and monitoring [26–28]. A recent study [29] discussed SSS image augmentation for sediment classification; the results indicate that the pretrained EfficientNet model improves accuracy after fine-tuning the parameters in feature identification and object classification using SSS images. A study [30] confirmed that the segmentation method based on conventional neural networks (CNNs) and Markov random fields (MRFs) is applicable in SSS image segmentation. Some researchers [31] combined semisynthetic data generation and deep transfer learning, which has proven to be an effective way to improve the accuracy of underwater object classification. The authors of [32] presented textural analyses of SSS images from Stanton Banks on the continental shelf off Northern Ireland. They detected faint trawling marks and differentiated between the different types of seafloor. A study [33] discussed an automated pipeline for identifying sites of archaeological interest off the coast of Malta from SSS images collected by an autonomous underwater vehicle (AUV). Their algorithm achieved precision and recall of up to 29.34% and 97.22%, respectively, which indicated a high number of false positives and that the model is good at identifying most of the positive instances, respectively. Based on the above literature review, the main contributions and work of this study are as follows:

1. This automation significantly improves the efficiency and accuracy of SSS image analysis, overcoming the traditional challenges of manual interpretation, which is time-consuming and subject to human error in dredge pit sedimentary environments.
2. A pit wall collapse could threaten the safety of ambient pipelines and platforms. The combination of the EGC model and SSS images is a promising tool for future dredge pit geomorphic feature evolution and hazards related to dredging.
3. As the first dredge-pit wall collapse SSS images, they could be used in other environments for hazard monitoring.

2. Sandy Point Dredge Pit Dataset and Effective Geomorphology Classification Model

2.1. Sandy Point Dredge Pit Dataset

In this section, we first introduce the area of interest. Then, the data collection process is explained, and multiple data augmentation techniques used for the training of deep learning models are presented.

2.1.1. Study Area

The Sandy Point dredge pit, situated 20 km west of the modern Mississippi River bird-foot delta, reaches a depth of about 18 m post-dredging, contrasted with the surrounding water's depth of approximately 11 m (Figure 1). This pit originated from a paleo-sandy river channel covered extensively by muddy deposits [7]. The nearby fluvial deposits from Grand Pass in the Mississippi Delta, about 12.5 km northeast of the pit, influence its shape and dynamics significantly. Over time, sediment dispersal from the Mississippi River has led to a seabed predominantly composed of mud around the Sandy Point pit area. Specifically, the bottom sediment composition here is 90% mud (particles finer than 63 μm) and 10% sand, contributing to its unique characteristics [7].

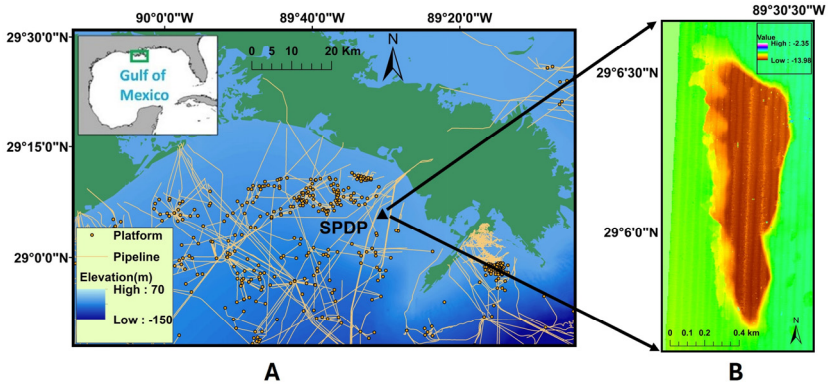

Figure 1. Map of the Mississippi bird-foot delta. (**B**) Bathymetry map for Sandy Point dredge pit. Bathymetric data for (**A**) are downloaded from ETOPO1 (https://www.ngdc.noaa.gov/mgg/global/, accessed on 12 July 2022). Oil platform and pipeline data are from BOEM website (https://www.data.boem.gov/, accessed on 12 July 2022). Bathymetric data for Sandy Point dredge pit were collected in May 2022 by [19]. 'SPDP' stands for Sandy Point dredge pit.

2.1.2. Data Collection

To collect the Sandy Point dredge pit (SPDP) dataset, we surveyed the Sandy Point dredge pit in September 2022 using a full suite of high-resolution geophysical instruments, including an interferometric sonar for swath bathymetry, a sidescan sonar, and a CHIRP subbottom profiler. A bow-mounted Edgetech 4600 interferometric swath bathymetry and sidescan sonar system was used to collect data with a swath width about 3–5 times the water depth. The 4600 system produces real-time, high-resolution, three-dimensional maps of the seafloor while providing co-registered simultaneous sidescan and bathymetric data. Seafloor features such as pit edges, failure scarps, and bedforms as small as 10–20 cm can be imaged. The R/V Coastal Profiler from the Coastal Studies Institute of Louisiana State University was used for all fieldwork. The bathymetry and sidescan acquisition devices were pole-mounted and fixed on a bowsprit ahead of the vessel. Additionally, we also used a motion sensor to record high-resolution data on ship motion. The subbottom profiler was towed off the port side of the vessel, about 0.5 m below the sea surface. Sonar data were processed using Caris HIPS/SIPS and then exported to ArcMap to create Digital Elevation Models (DEMs), which were then used to crop the original SSS images. The detailed geophysical methods can be found in [20]. After an initial data analysis, a total of five classes of environments were defined: pit wall with a rotational slump, pit wall without a rotational slump, heterogenous pit bottom (sand–mud mixture), homogenous pit

bottom, as well as homogenous seabed outside the pit. A rotational slump, also known as a rotational slide or rotational landslide, is a type of landslide that occurs along the pit wall of the SPDP. During a rotational slump, a series of blocks of sediment slide along a concave-upward slip surface, forming a stepwise boundary on the pit wall. It should be noted that black and white represent high and low reflectivity, respectively, in all SSS images in this study. Also, a close distance from the SSS to the seabed and sand seabeds tend to produce high reflectivity (i.e., black in SSS images).

The labeling rationale is mainly based on the bathymetry data collected at the same time, which makes it much easier to determine morphological features. More details are in Figure 2. After class definition, we applied a data preprocessing pipeline to the original data, as shown in Figure 3. Specifically, the original data were processed by augmentation techniques such as rotation, translation, scaling, and cropping to simulate the various data collection environments and enlarge the dataset size [34]. After data cleaning, a total of 385 SSS images were used, categorized into five classes. Specifications for the SPDP are given in Table 1.

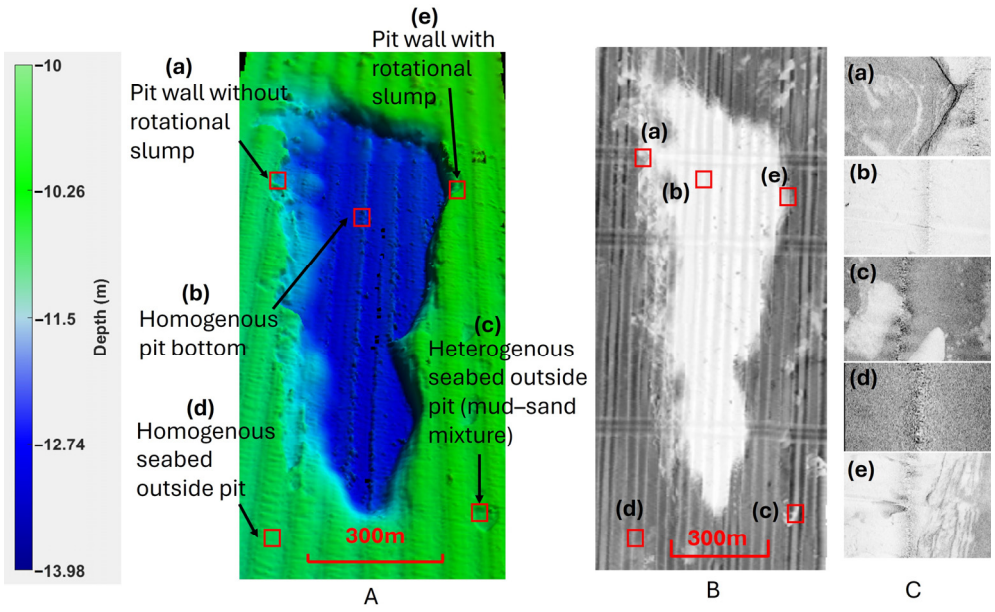

Figure 2. (**A**) is the bathymetry data of the Sandy Point dredge pit. (a)~(e) are the five feature categories highlighted as red squares. (**B**) is the whole sidescan data picture. (**C**) are samples of data from each feature category. The red squares are the samples' locations in the SSS images.

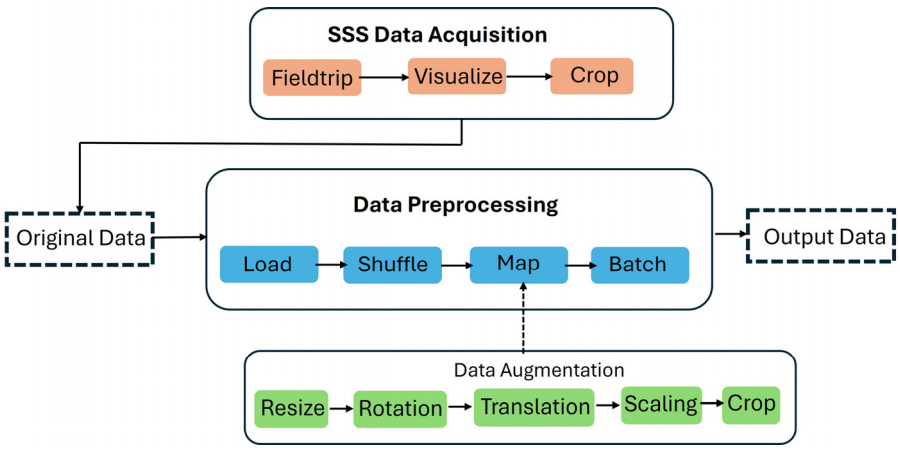

Figure 3. Data preprocessing flow chart. Multiple data augmentation techniques were applied to increase the diversity of the data and prepare the model for training.

Table 1. Specifications of SPDP dataset.

Class	Training	Validation	Total
Pit wall without rotational slump	28	7	36
Homogenous pit bottom	41	14	55
Heterogenous seabed outside pit (mud–sand mixture)	97	20	117
Homogenous seabed outside pit	78	15	93
Pit wall with rotational slump	64	21	84

2.1.3. Data Augmentation

In addressing the challenges posed by the limited size of our dataset, we implemented a strategic data preprocessing pipeline to enhance the diversity of our training samples, as shown in Figure 3. This process not only aided in increasing the effective size of our dataset but also played a crucial role in improving the generalizability of our model. Below, we detail the components of our data augmentation strategy and its integration into the data preprocessing workflow.

Preprocessing and Rescaling. Initially, all images in the dataset underwent a uniform resizing and rescaling operation. Specifically, the images were resized to standard dimensions of 224 × 224 pixels, which are commonly adopted image sizes [35]. Subsequently, pixel values were normalized to a range of 0 to 1 by rescaling with a factor of 1/255. This normalization step is critical for optimizing the training process, as it ensures that model inputs have a uniform scale, facilitating faster convergence during training.

Augmentation Techniques. To further enhance the robustness of our model, we employed a series of random transformations on the training dataset. These transformations, which included random flipping, random rotation, and random contrast adjustments, introduced a variety of perspectives and lighting conditions, simulating a broader range of real-world data collection scenarios:

1. Random Flipping: Images are randomly flipped horizontally or vertically.
2. Random Rotation: We apply a rotation range of $[-36°, 36°]$ to the images to account for changes in object positioning and camera angle.
3. Random Contrast: Adjustments in contrast (up to 10%) are made to simulate different lighting conditions.

For augmentation, the model transformed the images differently each time they passed through the augmentation pipeline during training. This means each epoch could see slightly different versions of the same image, which helped the model generalize better from the training data by preventing it from memorizing exact details. These augmentation techniques were applied exclusively to the training set, ensuring that the model learned from a more diverse set of examples without altering the test sets. Examples of augmented images are shown in Figure 4.

After random augmentations, the SSS image samples were randomly shuffled to further enhance model robustness by preventing the model from learning unintended patterns from the order of the samples. Finally, the images were divided into multiple batches according to the hyperparameter batch size.

2.2. Effective Geomorphology Classification Model

Although data augmentations are beneficial to increase the variety of data, our SPDP dataset still presents unique challenges to the design of the classification model due to its relatively small size and unique and intricate features. These features are often subtle yet critical for accurate classification, requiring a model that can learn effectively from limited data without overfitting. Additionally, the new model we need for this study should also have good training efficiency and scalability. Good training efficiency allows faster model training and inference and can even achieve real-time inference when conducting image collection at the same time. Good scalability allows customized model design for various sizes of available data, which is crucial for small and unique datasets like ours. Therefore,

we introduce an Effective Geomorphology Classification model (EGC), which aims to balance model performance and efficiency.

In this section, we first introduce the architecture of our EGC model. Then, we introduce the two main modules of the EGC in detail: the feature extractor and the classifier.

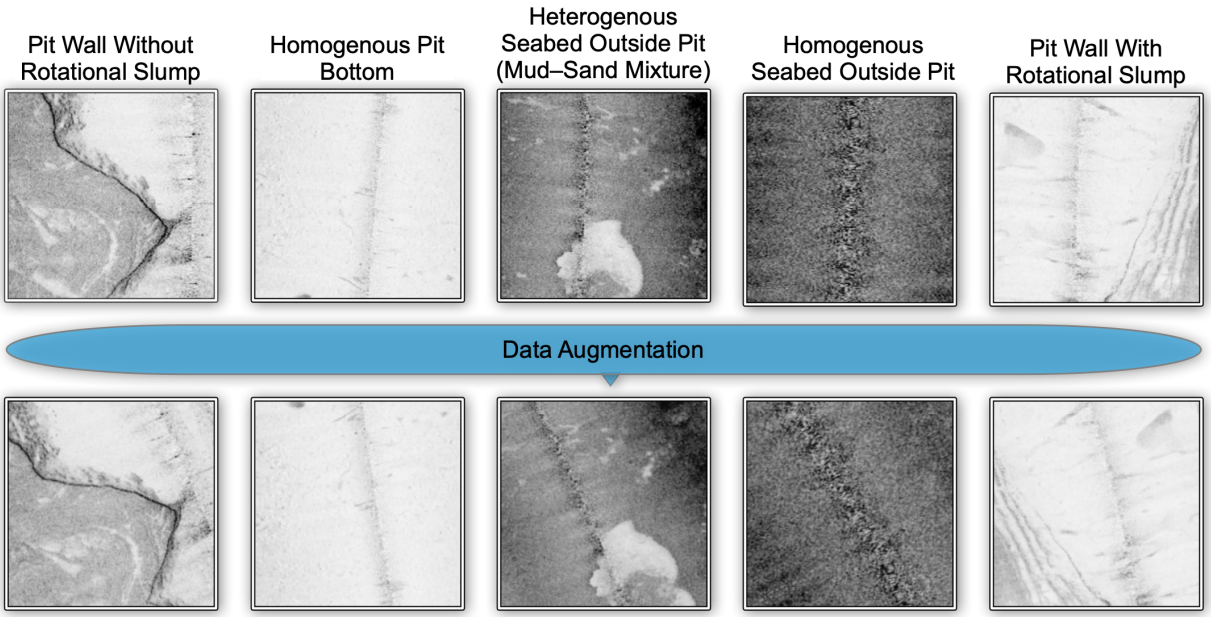

Figure 4. Examples of original and augmented images in five classes. The **top row** shows the original images, and the **bottom row** shows randomly augmented images. A total of 5 classes of environments were defined: pit wall with rotational slump, pit wall without rotational slump, heterogenous pit bottom (sand–mud mixture), homogenous pit bottom, as well as homogenous seabed outside the pit.

2.2.1. Model Architecture

To balance model performance and computational efficiency, we introduce an EGC model based on EfficientNet [36]. EfficientNet has shown good performance on image classification tasks with a great tradeoff between accuracy and training and inference efficiency, which is achieved by its innovative scaling approach. The EGC mainly has two modules: the feature extractor, which adopts EfficientNet-B0 as the backbone to extract various levels of grains of geomorphological features, and the classifier, which consists of two fully connected (FC) layers to perform predictions on five classes. The architecture of the EGC is shown in Figure 5.

As shown in Figure 5, the EGC is divided into 10 stages, and all the layers in each stage have the same architecture. Stages 0–7 are the components of the feature extractor module, and stages 8–9 are the layers of the classifier module.

2.2.2. Feature Extractor Module

The foundation of our EGC is the feature extractor module, which meticulously processes the input sidescan sonar images to distill meaningful patterns. This module is designed to handle the nuances of underwater imagery with a good balance between model performance and model size. Two major convolution blocks were utilized in the feature extractor module: MBConv and Fused-MBConv, as shown in Figure 6. MBConv is the main convolution block in MobileNet [37], which consists of two convolution layers with a kernel size of 1×1 and a depthwise block. Fused-MBConv is a variant of MBConv designed to achieve better training speed by replacing the depthwise conv3×3 and expansion conv1×1 in MBConv with a conv3×3 layer.

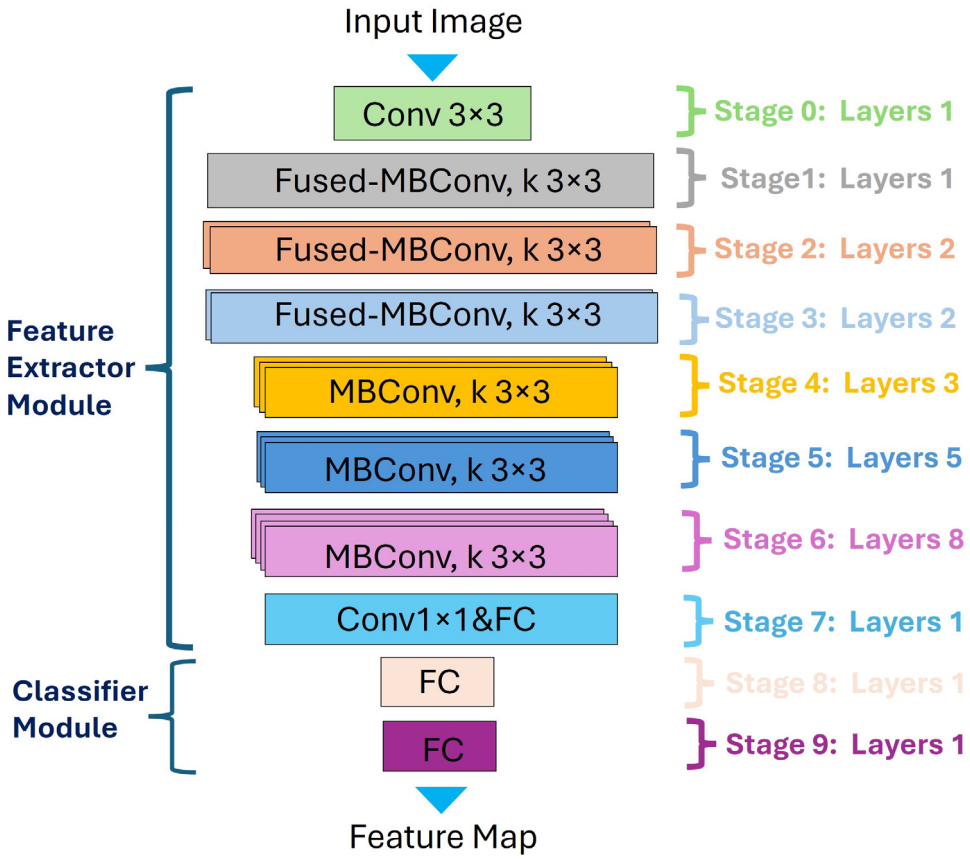

Figure 5. Model architecture of EGC.

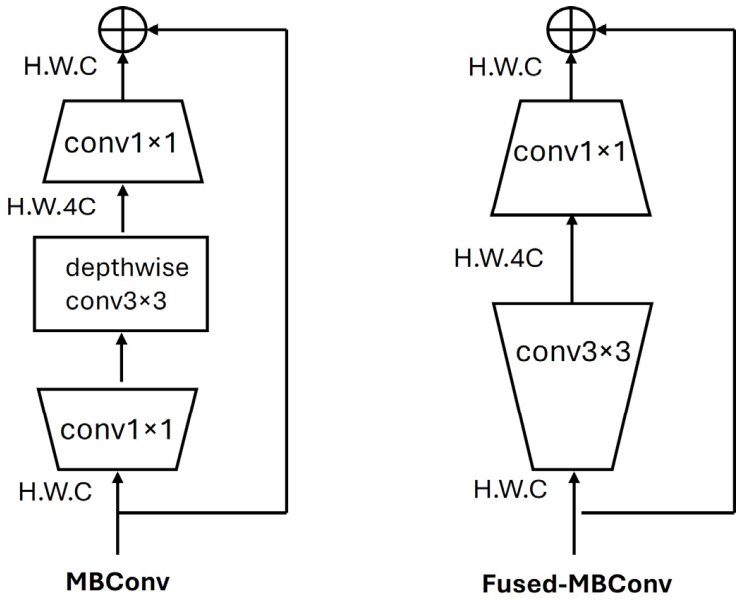

Figure 6. Structures of MBConv and Fused-MBConv blocks.

As shown in Figure 6, the feature extractor module begins with a standard convolutional layer (conv3 × 3) that is equipped with 32 filters of size 3 × 3 and has 32 channels. This serves as the initial feature extractor for the processed input images. The subsequent stages, 1 through 3, implement Fused-MBConv blocks. Fused-MBConv fuses the depthwise and pointwise convolutions into one layer for efficiency. They employ 3 × 3 kernels and exhibit increasing complexity in terms of the number of channels, starting at 16 and pro-

gressing to 48. Each stage incrementally captures more complex features while managing computational efficiency. Stages 4 to 6 integrate MBConv blocks with 3 × 3 kernels. The number of channels in these layers progressively increases from 96 to 192, allowing the network to construct a highly detailed feature representation from the input data. Finally, a regular conv1 × 1 and fully connected layer generates the output with a vector of 1280 dimensions.

2.2.3. Classifier Module

The classifier module contains two fully connected layers, where the output of the last layer is a vector of five dimensions, which corresponds to the number of classes in the geomorphology classification task.

Throughout the model, the number of layers within each stage varies, signifying the network's complexity and depth at different levels of abstraction. This hierarchical structure enables the model to effectively learn both low- and high-level features.

2.2.4. Experimental Settings

In our experiments, our batch size was set to 8. The total number of training epochs was 400. We used Adam [38] as the optimizer, where a cosine-decaying learning rate scheduler is applied with an initial learning rate of 0.001 and exponential decay rates of 0.9 and 0.999, respectively.

To evaluate the performance of our model, we utilized the top-1 accuracy metric. This metric is a direct measure of the model's ability to correctly classify the primary sediment type from an image, providing a clear and interpretable assessment of the classification performance.

To evaluate the classification performance of our EGC model, we selected a range of CNN architectures as backbones and connected them with the classifier module, each with varying complexities and characteristics. The specifications of the baselines are shown in Table 2.

Table 2. Specifications of the models. The number of parameters and float-point operations (FLOPs) is expressed in millions.

Model	#Parameter (M)	#FLOPs (M)
LeNet	0.005	20.00
VGG16	14.78	49.60
MobileNet Small	1.01	1.97
MobileNet Large	3.12	9.10
EGC	6.08	20.00

4. LeNet [39]: One of the earliest convolutional networks, LeNet is renowned for its simplicity and effectiveness in image classification tasks.
5. VGG16 [35]: A deep CNN renowned for its simplicity and depth that has shown exceptional performance on various image recognition tasks.
6. MobileNet [37] (Small and Large variants): MobileNet architectures are designed for mobile and edge devices, emphasizing efficiency. The 'Small' variant represents a more compact version, while the 'Large' variant is a scaled-up version with a higher capacity for feature extraction.

As shown in Table 2, our EGC has a medium size among the baselines and a moderate number of FLOPs. The design of the EGC balances training efficiency and model performance. Therefore, to fully evaluate the effectiveness of the EGC on our small dataset, we need to further measure its prediction performance in the following sections.

3. Results

3.1. Experimental Results

In this section, we present the major findings regarding the performance of our EGC model and ablation studies on some key components. All the experimental results presented are averaged from five independent experiments.

3.1.1. Model Performance

Typically, training CNNs from scratch where all the parameters of the model are trainable on small datasets is difficult because CNNs usually have a vast number of parameters that require substantial amounts of data to learn effectively without overfitting. When data are scarce, the model may not encounter enough variation to generalize well, leading it to memorize the limited training examples rather than learning the underlying patterns.

In this section, to evaluate the classification performance of our EGC model against the baselines, we train each baseline model from scratch. The accuracy and convergence speed are shown in Table 3, and the training curves are given in Figure 7.

Table 3. Classification performance and convergence speed of different models. Acc. denotes the best validation accuracy, and Converge Epoch denotes the number of epochs required to achieve 0.80 validation accuracy. The best result is in bold.

Model	Acc.	Converge Epoch (Efficiency)
LeNet	0.66	/
VGG16	0.26	/
MobileNet Small	**0.85**	216 (2.25×)
MobileNet Large	0.84	264 (2.75×)
EGC	0.82	**96 (1×)**

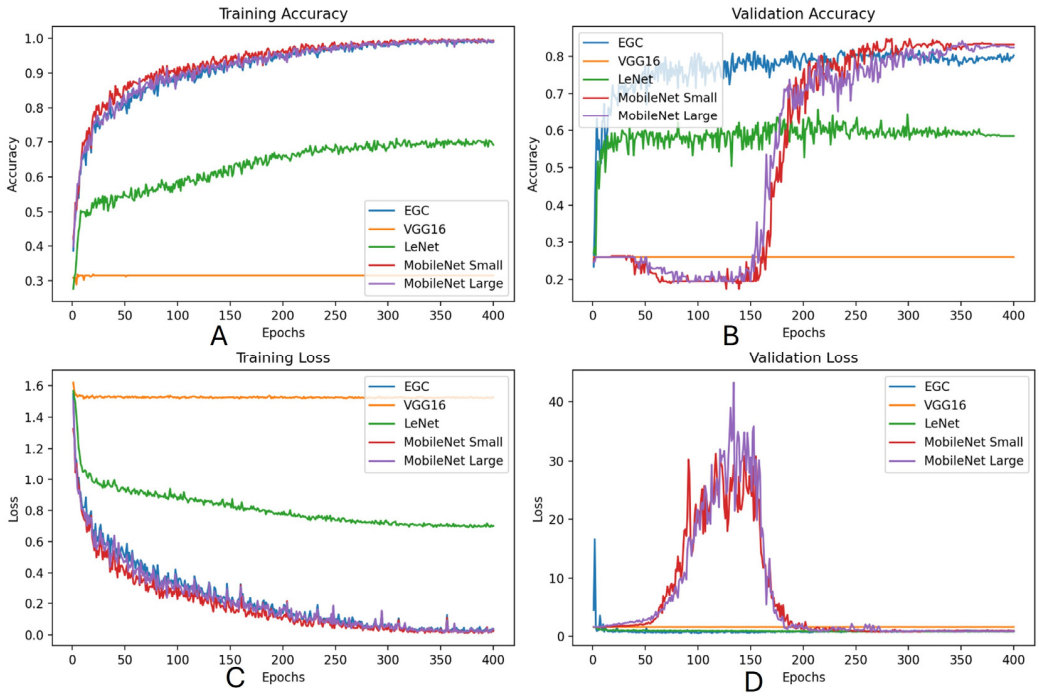

Figure 7. Performance of our EGC model against multiple baselines.

As shown in Figure 7, from the training accuracy and training loss curves, the EGC, along with MobileNet Small and MobileNet Large, converges fast and reaches the performance plateau with more than 0.95 accuracy at about epoch 200, while LeNet and VGG16 converge to the local minimum (Figure 7A,C). This indicates that LeNet and VGG16

are underfitting and not able to effectively extract the key features from our sidescan sonar images.

As shown in Table 3, the EGC has a significantly fast convergence speed and good generalization ability, achieving a stable validation accuracy of 0.80 after only 96 epochs of training. Although MobileNet Small and MobileNet Large have slightly higher accuracy than the EGC after 300 epochs of training, they are much less robust than the EGC with high fluctuations between epochs, as shown in Figure 7B. Moreover, MobileNet variants need a warmup of about 150 epochs to improve their validation accuracy, which shows significantly low training efficiency (Figure 7B).

3.1.2. Model Trained from Scratch versus Pretrained Model

The decision to train a CNN from scratch or to employ transfer learning of a model pretrained on a large dataset is critical to the success of model training, especially when faced with a small dataset. In this section, we evaluate the performance of two variants of our EGC model: EGC, trained from scratch, and EGC (Pretrained), which leverages transfer learning. Specifically, the feature extractor module of EGC (Pretrained) is pretrained on ImageNet, which is a vast and diverse image dataset, and the weights of the feature extractor are fixed, which leaves only the classifier to be updated on our SPDP dataset.

It is worth noting that we also apply transfer learning to other baselines. However, only VGG16 (Pretrained) shows good performance and reveals some interesting findings. Therefore, we add VGG16 and VGG16 (Pretrained) to the comparison. The results are shown in Figure 8.

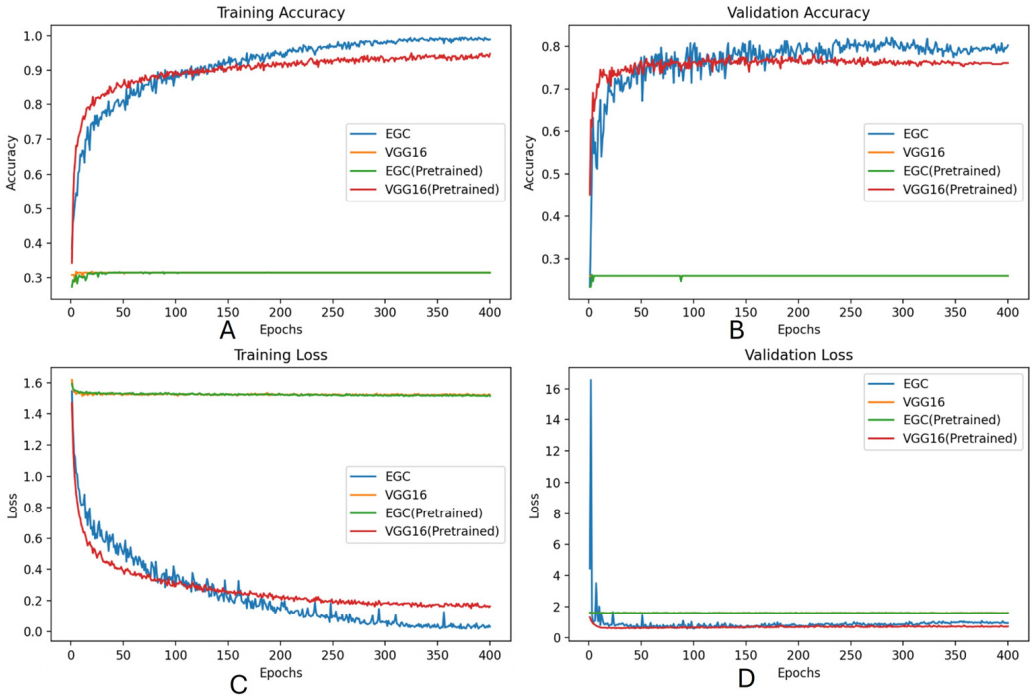

Figure 8. Performance comparison between EGC, EGC (Pretrained), VGG16, and VGG16 (Pretrained).

The EGC model, trained from scratch, demonstrates exceptional validation accuracy, with a training accuracy of up to 1.0 and a validation accuracy of up to 0.82, indicating that its architecture is well suited for the nuances of the dataset at hand (Figure 8B). Its superior performance suggests that, even without the benefits of transfer learning, the model is capable of learning robust and discriminative features specific to geomorphology classification.

Both VGG16 and EGC (Pretrained) exhibit signs of underfitting, as seen from their lower training accuracies (Figure 8A,B). In the case of VGG16, this could be attributed to its depth and the large number of parameters, which may be difficult to train effectively without a sufficiently large dataset. For the pretrained EGC, underfitting could be due to

the significant domain shift between natural images in ImageNet and the sonar imagery in our dataset. The model may struggle to adjust these features to the new task during fine-tuning, leading to poor performance in both the training and validation phases.

Complex models like VGG16, known for their performance on large and diverse datasets, may not always be the optimal choice for smaller, domain-specific datasets. For these models, transfer learning is beneficial because of the reduced number of trainable parameters. Instead, more specialized architectures like our EGC can capture the essential features effectively without transfer learning.

3.1.3. Ablation Study on Image Processing

In this ablation study, we investigate the impact of data preprocessing on the performance of our EGC model. By comparing the EGC with and without these preprocessing steps, we aim to understand their contribution to the model's learning efficacy. The results are shown in Figure 9.

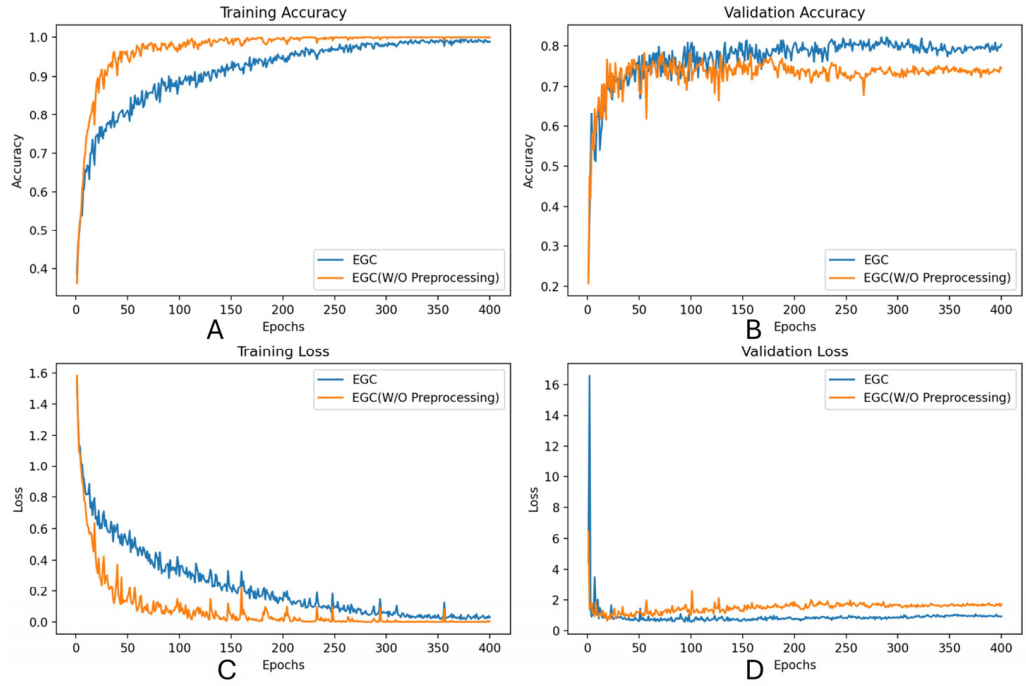

Figure 9. Performance comparison between EGC and EGC (W/O Preprocessing).

EGC is more resistant to overfitting and shows better generalization ability. Although EGC (W/O Preprocessing) initially exhibits a more rapid convergence during the early epochs of training, it begins to overfit after approximately 50 epochs, as evidenced by the divergence of training and validation loss (Figure 9C,D). Moreover, the EGC model, incorporating preprocessing steps, maintains steadier convergence and achieves higher validation accuracy by a large margin of 0.1 (Figure 9B). Overall, EGC shows better resistance to overfitting and better generalization ability, benefiting from data processing.

4. Discussion

In response to sea-level rise and land subsidence, dredging is a global human activity aimed at restoring coastal environments and slowing down land loss. It is anticipated that more dredge pits will be formed in future decades in response to growing sand mineral needs. Detecting pit walls and calculating the distances from pit walls to oil and gas pipelines and platforms are critical to the safety of marine mineral management. The data generated by our EGC model can help decision makers to better evaluate the setback buffer distance from pit walls to oil and gas pipelines, which is currently about 304 m as used by the U.S. Bureau of Ocean Energy Management. Moreover, submarine landslides are a type

of geohazard widely found in marine environments and pose a threat to nearby oil/gas pipelines and submarine fiber cables. Our EGC model can also be adapted and applied to the detection of the walls of gullies and lobes formed in the areas of submarine landslides, which can be triggered by hurricane waves, earthquakes, and tsunamis. It can also be used to detect complex shipwrecks in coastal and marine environments.

Several machine learning studies related to dredging activities have been reported in recent years, including identifying sediment types and sand mining [40,41]. However, utilizing machine learning methods to identify geomorphic features like dredge pit walls is still very limited. In September 2022, for example, some researchers [19] observed large submarine landslides on the west wall of the Sandy Point dredge pit (Figure 1). This was the first time that landslides occurred in dredge pits in muddy environments. This phenomenon has great implications for the safety of ambient gas and oil pipelines and platforms, as well as submarine fiber cables. Sand mineral management and dredging-related hazards require fast and efficient machine learning tools.

Compared with bathymetry and coring methods, sidescan sonar data are cheaper to collect and easier to process. Sidescan data are also excellent at detecting the edges and boundaries of contrasting seafloor objects. In recent years, a large amount of SSS data have been collected in coastal marine environments. Therefore, the combination of SSS data and machine learning is a promising method to monitor the geomorphic evolution of dredge pits and to study geohazards triggered by dredging activities. In this study, the EGC shows an excellent balance between model performance and training efficiency. Furthermore, it learns effectively from a relatively small dataset (Figure 7). The EGC model introduced in this study is promising to identify geomorphic features and even artificial infrastructure like oil platforms, pipelines, and the foundations of wind turbines in marine environments. This EGC model can be used for geomorphic feature identification and hazard monitoring in both sandy and muddy environments on the Louisiana continental shelf and even in other dredge pits around the world. Furthermore, marine dredging pit environments are on a relatively small spatial scale of 0.1 to several km. On a larger spatial scale of tens to hundreds of km, marine geomorphic features like shorelines, marsh edges, reef edges, delta fronts, continental shelf breaks, submarine canyons, seamounts, and guyots can also be identified. This model could be used to detect similar geomorphic features in a larger dataset or to monitor the temporal evolution of these features. Furthermore, submarine sediment transport could lead to significant erosion and deposition on the seabed during energetic events like hurricanes and storms. This often leads to the exposure of previously buried gas or oil pipelines on the seabed. Our EGC model can be used to detect the boundaries of metal pipes and mineral sediment and to identify the location of pipeline exposure. Thus, our EGC model will eventually benefit energy and environmental management in the marine environment.

5. Constraints and Future Work

The EGC model has limitations in identifying geomorphic features in dredge pit environments (see Figure 10). This could be a result of the small dataset and the complexity of geomorphic features. For example, Figure 10E shows an incorrect prediction, which is likely because the pit wall fraction is too small and quite different from a typical pit wall. Figure 10G,H present a similar problem. Additionally, Figure 10F yielded a wrong prediction because data noise makes the collapse feature incomplete and unpredictable. Therefore, in the future, creating a bigger SSS image dataset and conducting more training could make the EGC model robust and accurate. Moreover, a model specialized in identifying types of geomorphic features could be developed based on our EGC model.

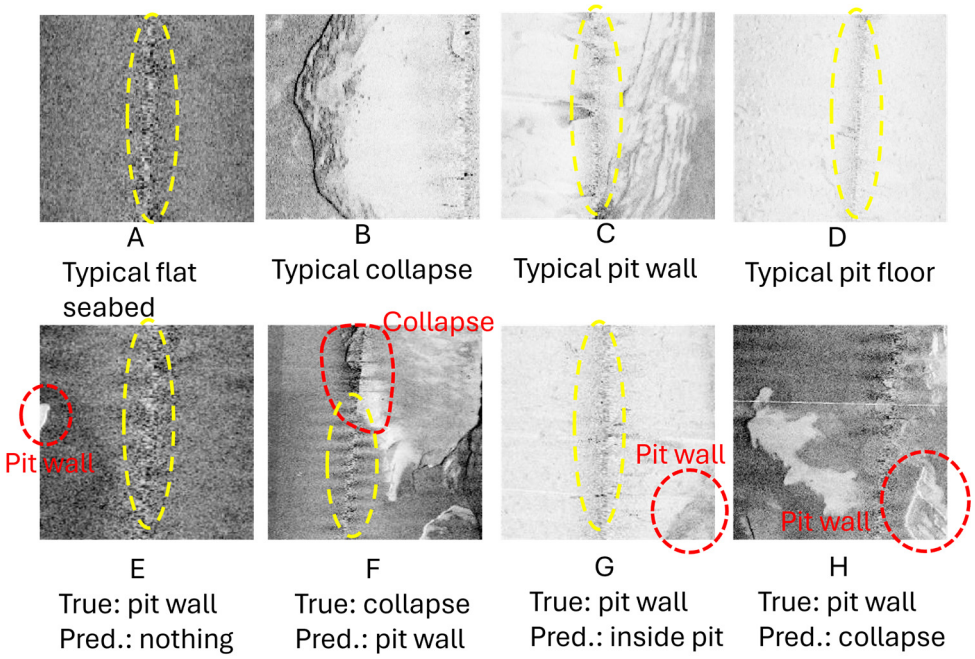

Figure 10. (**A**–**D**) are examples of typical features. (**E**–**H**) are examples of wrong predictions. The red dashed circles highlight the target features. The yellow dashed circles highlight the noise produced in the nadir of the SSS during data collection.

6. Conclusions

The use of machine learning models to identify geomorphic features from high-resolution SSS images is discussed in this study. The major conclusions are as follows:

1. Our EGC model was introduced to identify geomorphic features in marine dredge pit environments. The EGC model has the best training accuracy and validation accuracy when compared with several other machine learning models. Additionally, the EGC shows a better balance between model performance and training efficiency. Compared to other models, the EGC model trained from scratch has superior validation accuracy without transfer learning. The EGC model with preprocessing is more resistant to overfitting and shows better generalization ability.

2. Dredging-induced submarine landslides are a threat to the ambient energy and fiber cable infrastructure on the inner Louisiana continental shelf. The EGC model could be used to monitor landslides in dredge pits. Compared to the bathymetry data, SSS images are more cost-effective. The combination of SSS images and machine learning models (e.g., the EGC) could be a promising tool for monitoring geomorphic evolution and landslides in dredge pit environments. Moreover, the EGC model introduced in this study and the comprehensive SSS image dataset are valuable to future machine learning studies.

Author Contributions: Conceptualization, W.Z. and K.X.; formal analysis, W.Z., X.C. and K.X.; funding acquisition, K.X.; methodology, W.Z. and X.C.; software, W.Z. and X.C.; visualization, W.Z. and X.C.; writing—original draft, W.Z. and X.C.; writing—review and editing, K.X., X.Z., J.C., J.Y. and T.Z. All authors have read and agreed to the published version of the manuscript.

Funding: This study was funded by the Bureau of Ocean Energy Management Agreement Number M14AC00023 and multiple others, with Barton Rogers, Christopher DuFore, and Michael Miner serving as project officers of the Bureau of Ocean Energy Management. This study was also partly funded by the U.S. Coastal Research Program (W912HZ2020013) and the National Science Foundation RAPID program (2203111).

Institution Review Board Statement: Not applicable.

Informed Consent Statement: Not applicable.

Data Availability Statement: The data presented in this study are available on request from the corresponding author. The data are not publicly available due to confidentiality.

Conflicts of Interest: The authors have no conflicts of interest.

References

1. Penland, S.; Suter, J.R. Barrier island erosion and protection in Louisiana: A coastal geomorphological perspective. *Gulf Coast Assoc. Geol. Soc. Trans.* **1988**, *38*, 331–342.
2. Penland, S.; Ramsey, K.E. Relative sea-level rise in Louisiana and the Gulf of Mexico: 1908–1988. *J. Coast. Res.* **1990**, *6*, 323–342.
3. Stone, G.W.; McBride, R.A. Louisiana barrier islands and their importance in wetland protection: Forecasting shoreline change and subsequent response of wave climate. *J. Coast. Res.* **1998**, *14*, 900–915.
4. Miner, M.D.; Kulp, M.A.; FitzGerald, D.M.; Flocks, J.G.; Weathers, H.D. Delta lobe degradation and hurricane impacts governing large-scale coastal behavior, South-central Louisiana, USA. *Geo-Mar. Lett.* **2009**, *29*, 441–453. [CrossRef]
5. Maloney, J.M.; Bentley, S.J.; Xu, K.; Obelcz, J.; Georgiou, I.Y.; Miner, M.D. Mississippi River subaqueous delta is entering a stage of retrogradation. *Mar. Geol.* **2018**, *400*, 12–23. [CrossRef]
6. Van Heerden, I.L.; DeRouen, K., Jr. Implementing a barrier island and barrier shoreline restoration program: The state of Louisiana's perspective. *J. Coast. Res.* **1997**, *13*, 679–685.
7. Nairn, R.; Johnson, J.A.; Hardin, D.; Michel, J. A biological and physical monitoring program to evaluate long-term impacts from sand dredging operations in the United States outer continental shelf. *J. Coast. Res.* **2004**, *20*, 126–137. [CrossRef]
8. Kulp, M.; Penland, S.; Williams, S.J.; Jenkins, C.; Flocks, J.; Kindinger, J. Geologic framework, evolution, and sediment resources for restoration of the Louisiana coastal zone. *J. Coast. Res.* **2005**, *44*, 56–71.
9. Brunn, P.; Gayes, P.T.; Schwab, W.C.; Eiser, W.C. Dredging and offshore transport of materials. *J. Coast. Res.* **2005**, *46*, 453–525.
10. Thomsen, F.; McCully, S.; Wood, D.; Pace, F.; White, P. *A Generic Investigation into Noise Profiles of Marine Dredging in Relation to the Acoustic Sensitivity of the Marine Fauna in UK Waters with Particular Emphasis on Aggregate Dredging: Phase 1 Scoping and Review of Key Issues*; Cefas MEPF Ref No; Fisheries & Aquaculture Science: Suffolk, UK, 2009; p. 61.
11. CEDA. CEDA position paper: Underwater sound in relation to dredging. *Terra Aqua* **2011**, *125*, 23–28.
12. Tillin, H.M.; Houghton, A.J.; Saunders, J.E.; Hull, S.C. Direct and Indirect Impacts of Marine Aggregate Dredging. *Mar. ALSF Sci. Monogr. Ser.* **2011**, *1*.
13. WODA, World Organization of Dredging Associations. *Technical Guidance on Underwater Sound in Relation to Dredging*; World Organization of Dredging Associations: Delft, The Netherland, 2013; 8p.
14. Todd, V.L.; Todd, I.B.; Gardiner, J.C.; Morrin, E.C.; MacPherson, N.A.; DiMarzio, N.A.; Thomsen, F. A review of impacts of marine dredging activities on marine mammals. *ICES J. Mar. Sci.* **2015**, *72*, 328–340. [CrossRef]
15. CEC; CECI. *NRDA Caminada Headland Beach and Dune Restoration, Increment II (BA-143) Completion Report*; State of Louisiana Coastal Protection and Restoration Authority: Baton Rouge, LA, USA, 2017.
16. Stone, G.W.; Condrey, R.E.; Fleeger, J.W.; Khalil, S.M.; Kobashi, D.; Jose, F.; Evers, E.; Dubois, S.; Liu, B.; Arndt, S.; et al. *Environmental Investigation of Long-Term Use of Ship Shoal Sand Resources for Large Scale Beach and Coastal Restoration in Louisiana*; OCS Study MMS; US Deparment of the Interior, Minerals Management Service, Gulf of Mexico OCS Region: New Orleans, LA, USA, 2009; Volume 24, p. 278.
17. Rangel-Buitrago, N.G.; Anfuso, G.; Williams, A.T. Coastal erosion along the Caribbean coast of Colombia: Magnitudes, causes and management. *Ocean. Coast. Manag.* **2015**, *114*, 129–144. [CrossRef]
18. Alawneh, O.; Jafari, N.; Zhang, W.; Xu, K. Geotechnical properties of dredge pits for barrier island restoration. In Proceedings of the Coastal Sediments, New Orleans, LA, USA, 11–15 April 2023; pp. 2383–2390.
19. Zhang, W.; Xu, K.; Herke, C.; Alawneh, O.; Jafari, N.; Maiti, K.; Clower, P.O.; Glaspie, C.N.; Tupitza, J.C.; Xue, Z.G. Spatial and temporal variations of seabed sediment characteristics in the inner Louisiana shelf. *Mar. Geol.* **2023**, *463*, 107115. [CrossRef]
20. Obelcz, J.; Xu, K.; Bentley, S.J.; O'Connor, M.; Miner, M.D. Mud-capped dredge pits: An experiment of opportunity for characterizing cohesive sediment transport and slope stability in the northern Gulf of Mexico. *Estuar. Coast. Shelf Sci.* **2018**, *208*, 161–169. [CrossRef]
21. Xu, K.; Corbett, D.; Walsh, J.; Young, D.; Briggs, K.; Cartwright, G.; Friedrichs, C.; Harris, C.; Mickey, R.; Mitra, S. Seabed erodibility variations on the Louisiana continental shelf before and after the 2011 Mississippi River flood. *Estuar. Coast. Shelf Sci.* **2014**, *149*, 283–293. [CrossRef]
22. Byrnes, M.R.; Hammer, R.M.; Thibaut, T.D.; Snyder, D.B. Physical and biological effects of sand mining offshore Alabama, USA. *J. Coast. Res.* **2004**, *20*, 6–24. [CrossRef]
23. Kennedy, A.B.; Slatton, K.C.; Starek, M.; Kampa, K.; Cho, H.C. Hurricane response of nearshore borrow pits from airborne bathymetric lidar. *J. Waterw. Port Coast. Ocean. Eng.* **2010**, *136*, 46–58. [CrossRef]
24. Denny, J.F.; Baldwin, W.E.; Schwab, W.C.; Gayes, P.T.; Morton, R.; Driscoll, N.W. *Morphology and Textures of Modern Sediments on the Inner Shelf of South Carolina's Long Bay from Little River Inlet to Winyah Bay (No. 2005-1345)*; US Geological Survey: Asheville, NC, USA, 2007.
25. Freeman, A.M.; Roberts, H.H.; Banks, P.D. Hurricane impact analysis of a Louisiana shallow coastal bay bottom and its shallow subsurface geology. *Gulf Coast Assoc. Geol. Soc. Trans.* **2007**, *57*, 255–267.

26. Reed, S.; Petillot, Y.; Bell, J. An automatic approach to the detection and extraction of mine features in sidescan sonar. *IEEE J. Ocean. Eng.* **2003**, *28*, 90–105. [CrossRef]
27. Celik, T.; Tjahjadi, T. A novel method for sidescan sonar image segmentation. *IEEE J. Ocean. Eng.* **2011**, *36*, 186–194. [CrossRef]
28. Barngrover, C.; Kastner, R.; Belongie, S. Semisynthetic versus real-world sonar training data for the classification of mine-like objects. *IEEE J. Ocean. Eng.* **2014**, *40*, 48–56. [CrossRef]
29. Chandrashekar, G.; Raaza, A.; Rajendran, V.; Ravikumar, D. Side scan sonar image augmentation for sediment classification using deep learning-based transfer learning approach. *Mater. Today Proc.* **2023**, *80*, 3263–3273. [CrossRef]
30. Song, Y.; Zhu, Y.; Li, G.; Feng, C.; He, B.; Yan, T. Side scan sonar segmentation using deep convolutional neural network. In Proceedings of the OCEANS 2017-Anchorage IEEE, Anchorage, AK, USA, 18–21 September 2017; pp. 1–4.
31. Huo, G.; Wu, Z.; Li, J. Underwater object classification in sidescan sonar images using deep transfer learning and semisynthetic training data. *IEEE Access* **2020**, *8*, 47407–47418. [CrossRef]
32. Blondel, P.; Sichi, O.G. Textural analyses of multibeam sonar imagery from Stanton Banks, Northern Ireland continental shelf. *Appl. Acoust.* **2009**, *70*, 1288–1297. [CrossRef]
33. Nayak, N.; Nara, M.; Gambin, T.; Wood, Z.; Clark, C.M. Machine learning techniques for AUV side-scan sonar data feature extraction as applied to intelligent search for underwater archaeological sites. In *Field and Service Robotics: Results of the 12th International Conference*; Springer: Singapore, 2021; pp. 219–233.
34. Shaisundaram, V.S.; Chandrasekaran, M.; Sujith, S.; Kumar, K.P.; Shanmugam, M. Design and analysis of novel biomass stove. *Mater. Today Proc.* **2021**, *46*, 4054–4058. [CrossRef]
35. Simonyan, K.; Zisserman, A. Very deep convolutional networks for large-scale image recognition. *arXiv* **2014**, arXiv:1409.1556.
36. Tan, M.; Le, Q. Efficientnet: Rethinking model scaling for convolutional neural networks. In Proceedings of the International Conference on Machine Learning PMLR, Long Beach, CA, USA, 9–15 June 2019; pp. 6105–6114.
37. Sandler, M.; Howard, A.; Zhu, M.; Zhmoginov, A.; Chen, L.C. Mobilenetv2: Inverted residuals and linear bottlenecks. In Proceedings of the IEEE Conference on Computer Vision and Pattern Recognition 2018, Salt Lake City, UT, USA, 18–23 June 2018; pp. 4510–4520.
38. Kingma, D.P.; Ba, J. Adam: A method for stochastic optimization. *arXiv* **2014**, arXiv:1412.6980.
39. LeCun, Y.; Bottou, L.; Bengio, Y.; Haffner, P. Gradient-based learning applied to document recognition. *Proc. IEEE* **1998**, *86*, 2278–2324. [CrossRef]
40. Liu, H.; Xu, K.; Li, B.; Han, Y.; Li, G. Sediment identification using machine learning classifiers in a mixed-texture dredge pit of Louisiana shelf for coastal restoration. *Water* **2019**, *11*, 1257. [CrossRef]
41. Kumar, S.; Park, E.; Tran, D.D.; Wang, J.; Ho, H.L.; Feng, L.; Kantoush, S.A.; Van Binh, D.; Li, D.; Switzer, A.D. A deep learning framework to map riverbed sand mining budgets in large tropical deltas. *GISc. Remote Sens.* **2024**, *61*, 2285178. [CrossRef]